International Journal of Multiphase Flow 35 (2009) 55–65

Contents lists available at ScienceDirect

International Journal of Multiphase Flow

journal homepage: www.elsevier.com/locate/ijmulflow

Surface tension effects on adiabatic gas–liquid flow across micro pillars

Santosh Krishnamurthy, Yoav Peles *

Department of Mechanical, Aerospace and Nuclear Engineering, Rensselaer Polytechnic Institute, 110, 8th Street, Troy, NY 12180, USA

ARTICLE INFO

Article history:
Received 5 February 2008
Received in revised form 6 July 2008
Accepted 13 August 2008
Available online 26 August 2008

ABSTRACT

The effect of surface tension on adiabatic two-phase flow across a bank of 100 μm diameter staggered circular micro pillars, 100 μm long with pitch-to-diameter ratio of 1.5, for Reynolds number between 5 and 50, was investigated. Experiments with ethanol were performed and compared to results with water. Flow maps revealed similar flow patterns, but the transition lines were different for the two liquids. Void fraction measurements of the two fluids were also compared, and no significant deviations were observed. The two-phase pressure drop characteristics were significantly affected by the reduction in surface tension. Interfacial friction was attributed to this deviation, and a two-fluid model was developed to account for surface tension force. In addition, a modified form of Chisholm correlation was developed that accounts for surface tension.

1. Introduction

Improvement of microfabrication techniques in the last decade has facilitated the design and fabrication of myriad micro flow domains for numerous microfluidic and microthermal applications. As a part of this effort, microchannels encompassing an array of micro-pillars for a range of applications, such as micro-chemical reactors (Losey et al., 2002), micro-rockets (Hitt et al., 2001; London, 2000), micro-biological systems (Christel et al., 1999), and micro-heat exchangers (Koşar and Peles, 2006, 2007; Siu-Ho et al., 2007), have been explored. Better knowledge of surface tension effects is important not merely from the fundamental stand point, but also to improve the design of many micro systems.

In conventional scale, the hydrodynamic characteristics of two-phase flow were extensively investigated and were found to primarily depend on inertial and gravitational forces (Grant and Chislom, 1979; Xu et al., 1998b; Dowlati et al., 1988; Dowlati et al., 1990; Dowlati et al., 1992b; Schrage et al., 1988; Xu et al., 1998a). In microscale, these flow characteristics significantly deviate from those observed in conventional scale, mainly because of the gradual dominance of surface tension and viscous forces, over inertial and gravitational forces (Kawahara et al., 2002; Chung and Kawaji, 2004; Kawaji and Chung, 2004; Cubaud and Ho, 2004; Krishnamurthy and Peles, 2007; Krishnamurthy and Peles, 2008)). Several new two-phase flow phenomena have been revealed, such as ring-slug/slug-ring flow in microchannels (Kawahara et al., 2002) and bridge flow in micro-pillar systems (Krishnamurthy and Peles, 2007). Void fraction and two-phase pressure drop were also altered at the micro scale. For example, the void fraction has been found to strongly depend on viscous forces for microchannels (Kawahara et al., 2002) (Dh = 100 μm) as well as for flow across micro pillars (Krishnamurthy and Peles, 2007). In mini-scale systems, the two-phase pressure drop has been successfully correlated by modifying the Chisholm correlation (Chisholm and Laird, 1949) to account for surface tension and viscous forces (Lee and Lee, 2001; Field and Hrnjak, 2007). For crossflows in micro-scale, Krishnamurthy and Peles (2007) accounted for the viscous effects by incorporating the Reynolds number in the C-parameter of a Chisholm-type correlation.

In micro domains, surface tension and viscous forces begin to dominate. However, much is unknown about the effect of fluid properties, such as surface tension and viscosity, on the two-phase flow characteristics in small length scales. Kawahara et al. (2005) in their study on gas–liquid flow in microchannel observed that the surface tension did not significantly affect the void fraction. Krishnamurthy and Peles (2007) investigated adiabatic flow across micro pillars and reported new surface tension dependent flow pattern and some unique two-phase flow characteristics. It was argued that the surface tension played a very important role in governing the flow hydrodynamics in cross flow systems.

In the current study, the effect of surface tension on two-phase flow across a staggered array of 100 μm diameter by 100 μm deep micro pillars entrenched inside microchannel was investigated. Section 2 provides a detailed overview of the device geometry and presents the essential microfabrication processes used. Additionally, an overview of the experimental setup and procedure is presented. Section 3 presents the methodology used for data reduction. The results and discussion section (Section 4) includes discussions on: (a) flow patterns and their transition, (b) void fraction, and (c) two-phase pressure drop. The physical mechanism governing the flow was modeled and a correlation was developed/modified to account for the

* Corresponding author.
E-mail address: pelesy@rpi.edu (Y. Peles).

0301-9322/$ - see front matter © 2008 Elsevier Ltd. All rights reserved.
doi:10.1016/j.ijmultiphaseflow.2008.08.001

effect of surface tension. Finally, the main conclusion of this study is presented in Section 5.

2. Device overview, fabrication and experimental setup

The following section gives a detailed over view of the device geometry and the pertinent microfabrication processes.

2.1. Device overview

A computer aided design (CAD) schematic of the device consisting of a 1500 μm wide and 1 cm long microchannel of depth 100 μm is shown in Fig. 1. The microchannel encompassed 68 alternating rows of 9 and 10 staggered circular 100 μm diameter pillars. A Pyrex cover sealed the device from the top and allowed flow visualization. Pressure taps were placed at the inlet, exit, and in three different locations along the device to enable pressure measurements. Upstream the main pillar arrays, gas and liquid entered a mixer and formed a well mixed two-phase flow. Unlike other studies in micro-scale by Kawahara et al. (2002), Chung and Kawaji (2004), where the two-phases were mixed externally before entering the test section, in the current study the mixer was fabricated as part of the device. The mixer has two inlets, one for liquid and one for nitrogen, and a series of closely spaced 50 μm diameter circular pillars with pitch-to-diameter ratio of 1.3. The design of the mixer was similar to that found in some conventional scale studies (e.g., Grant and Chislom, 1979).

2.2. Microfabrication process flow

A double side polished, n-type ⟨100⟩ single crystal silicon wafer was processed on both sides to create the microelectromechanical system (MEMS) device, which consisted of a microchannel enclosing the array of pillars. Prior to the fabrication process, the top side and bottom side masks were designed and fabricated. A 1 μm thick oxide was deposited on both sides of the silicon wafer to protect the bare wafer surface. Next, the microchannel with the micro-pillars was formed on the top side of the wafer. For this, the wafer was taken through a photolithography step and a reactive ion etching (RIE) oxide removal process to mask certain areas on the wafer, which were to be protected during the deep reactive ion etching (DRIE) process. The wafer was consequently etched in a DRIE process, and silicon was removed from places not protected by the photoresist/oxide mask. The DRIE process formed deep vertical trenches on the silicon wafer with a characteristic scalloped sidewall possessing a peak-to-peak roughness of ~0.3 μm. A profilometer and a scanning electron microscope (SEM) were employed to measure and record various dimensions of the device. The wafer was flipped and the backside was processed, to form the inlet, the exit, and the pressure port taps for the transducers. Photolithography followed by a buffered oxide etch (BOE) (6:1) oxide removal process was carried out to create a pattern mask. The wafer was then etched-through in a DRIE process to create the fluidic ports. Finally, the processed wafer was stripped of any remaining resist or oxide layers and anodically bonded to a 1 mm thick polished Pyrex (glass) wafer to form a sealed device. After successful

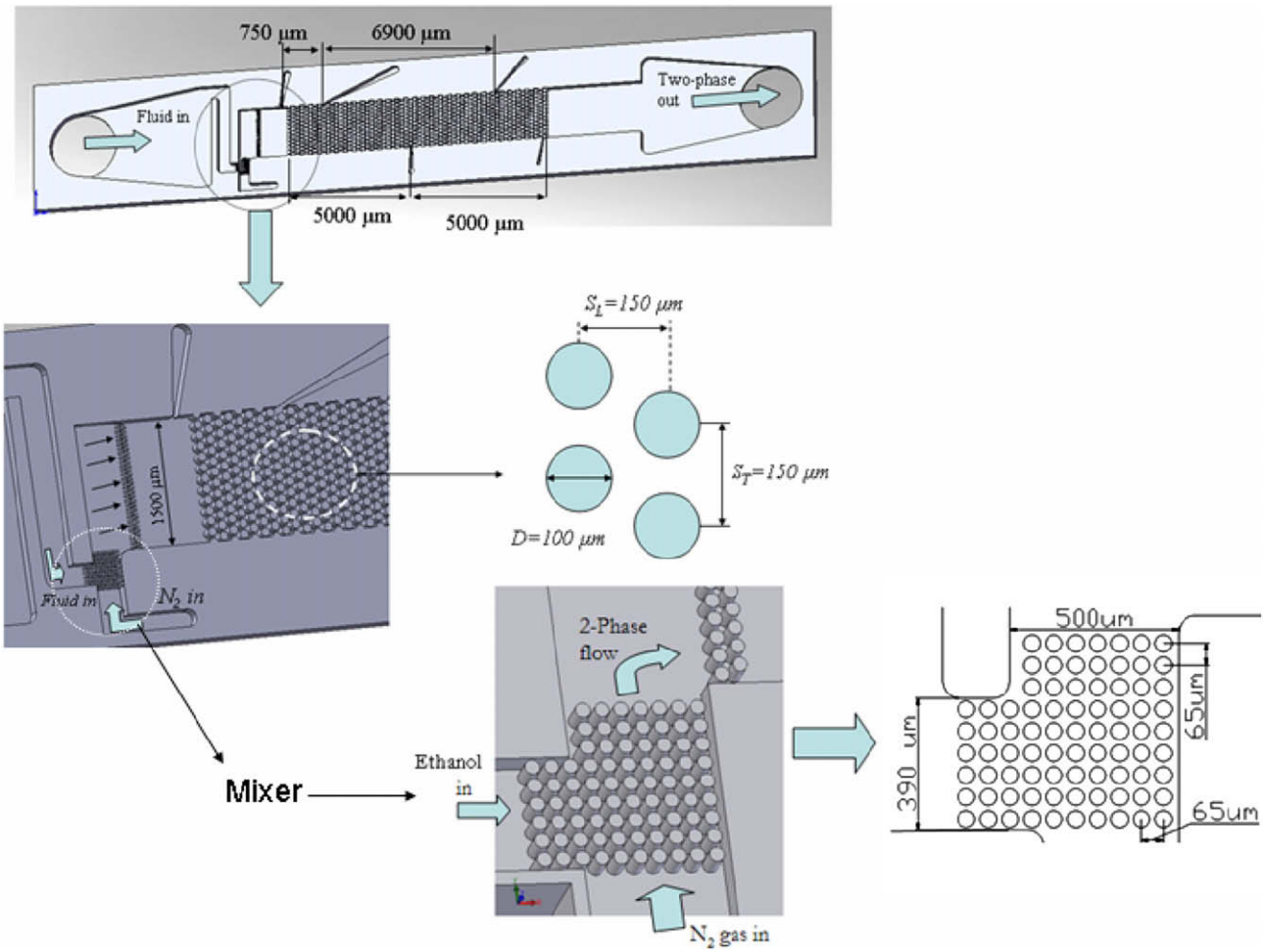

Fig. 1. The device overview showing the flow configuration.

completion of the bonding process, the processed stack was diesawed to separate the devices from the parent wafer.

2.3. Experimental apparatus and procedure

The schematic diagram of the experimental set up is shown in Fig. 2. The test section consisted of the device with pressure ports and a packaging module to facilitate the transit of fluids to the micro-device and also to record the pressure drop across the channels. The MEMS device was placed in the package by means of o-rings, which act as hermetic seals and connect the pressure ports and inlet/outlet of the channel to the flow loop. The liquid was delivered to the channel through a calibrated flow meter (Omega Engineering, Inc, FL-110 series), and a 0.2 μm filter was used to avoid clogging of the device. The liquid flow meter was capable of reading flow rates from 0 to 1.31 ml/min. Nitrogen (N_2) at desired pressure and flow rate was delivered to the channel through a 0.5 μm air filter and through a mass flow meter (Sierra Instruments, Inc, 820-S series) capable of measuring volumetric flow rates ranging from 0 to 50 ml/min. The gas meter was calibrated for pressures ranging from 101 and 414 kPa. Before passing the two-phase mixture through the channel, the entire channel was vacuumed to 10 kPa and then flooded with ethanol, including the pressure ports, to remove any gas bubbles trapped in the loop. After flushing the loop, nitrogen was allowed to enter the test section. Introducing the gas into the loop reduces the ethanol flow rate due to an increase in the hydraulic resistance. The valves of the N_2 and ethanol loop were iteratively controlled to obtain the desired gas and liquid flow rates. The pressure ports were connected to pressure transducers (Omega Engineering, Inc.), each capable of measuring pressures of up to 50 psia via the packaging module. Data from the pressure transducer was delivered to the PC based LabVIEW® program and stored in a file for further analysis. The images from the device were captured by means of high speed CMOS camera capable of capturing images up to 90,000 frames per second and a maximum resolution of 512×512 pixels. Images from five different locations along the channel were captured for processing void fraction measurements and identifying flow patterns. In order to distinguish gas from liquid, intensity threshold was applied to each image. Following, the area corresponding to the gas and liquid were calculated using Image-pro plus software. It should be noted that the intensity of the liquid and the pillars are of the same magnitude. Thus, for each image, the areas of the pillars were subtracted from the area of the liquid. The void fraction was then calculated as the ratio of the area of the gas to the total flow area. Any overlap between the liquid and the gas intensities were accounted for by manually calculating the overlapped region and applying a suitable correction to the measured areas. The contribution of the gas–liquid interface to the area was also accounted in determining the void fraction. The gas–liquid interface was approximated to have a circular profile as shown in Fig. 3. The volume of the liquid and gas phases in the interface was obtained by multiplying the area of the gas ($A_{\text{int,gas}}$) and the liquid ($A_{\text{int,liquid}}$) with the total length of the gas–liquid interface (l) in the xy plane. The total length of the interface was measured for every frame by using the Image pro plus software. The overall void fraction was then averaged over 20 frames using the following equation:

$$\alpha = \sum_{i=1}^{20} \frac{A_{gp}H + A_{\text{int,gas}}l}{V_{\text{total}}}, \quad i = \text{Number of the frame}, \tag{1}$$

where V_{total} is the total volume of the control volume, which is equal to the product of the projected area of the flow field in the xy plane (obtained through flow visualization) and the height of the microchannel. The comparison of the experimental data with existing models is performed through the mean absolute error (MAE):

$$\text{MAE} = \frac{1}{M}\sum_{i=1}^{M} \frac{|\theta_{\text{exp}} - \theta_{\text{pred}}|}{\theta_{\text{pred}}} \times 100 \tag{2}$$

where θ is the measured physical quantity and the subscripts 'exp' and 'pred' refer to experimental and predicted values, respectively. The uncertainty of measured experimental values are listed in Table 1 and are derived from the manufacturers' specification sheets while the uncertainties of the derived quantities are determined

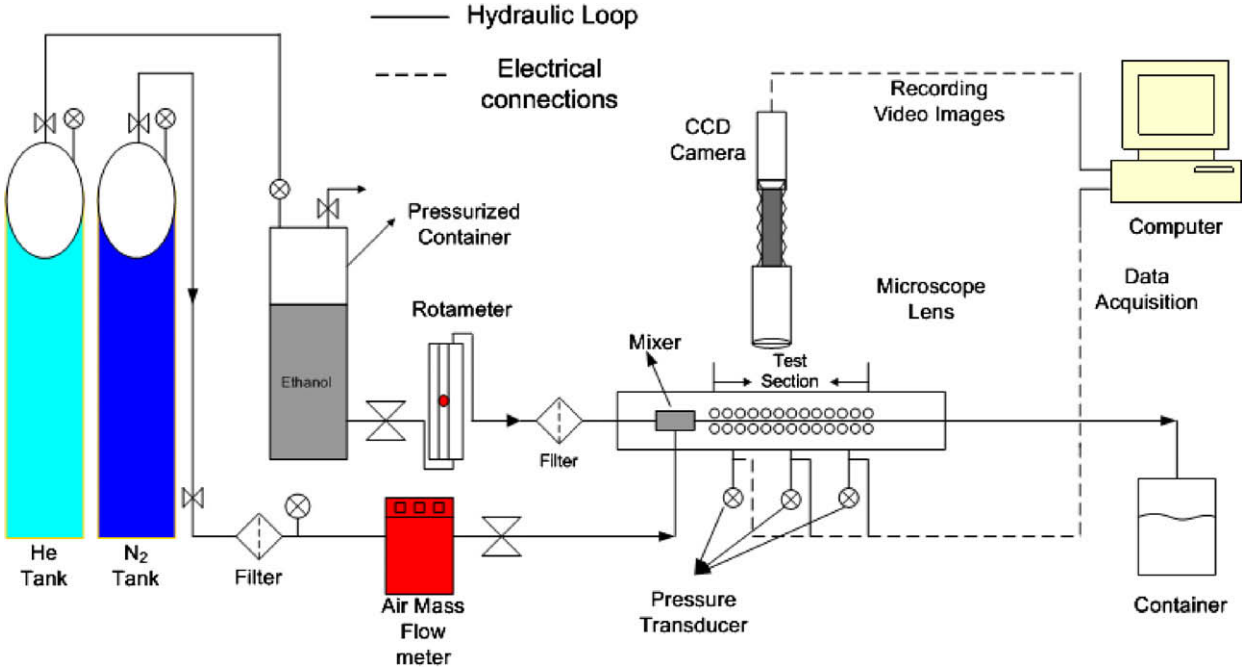

Fig. 2. The experimental setup.

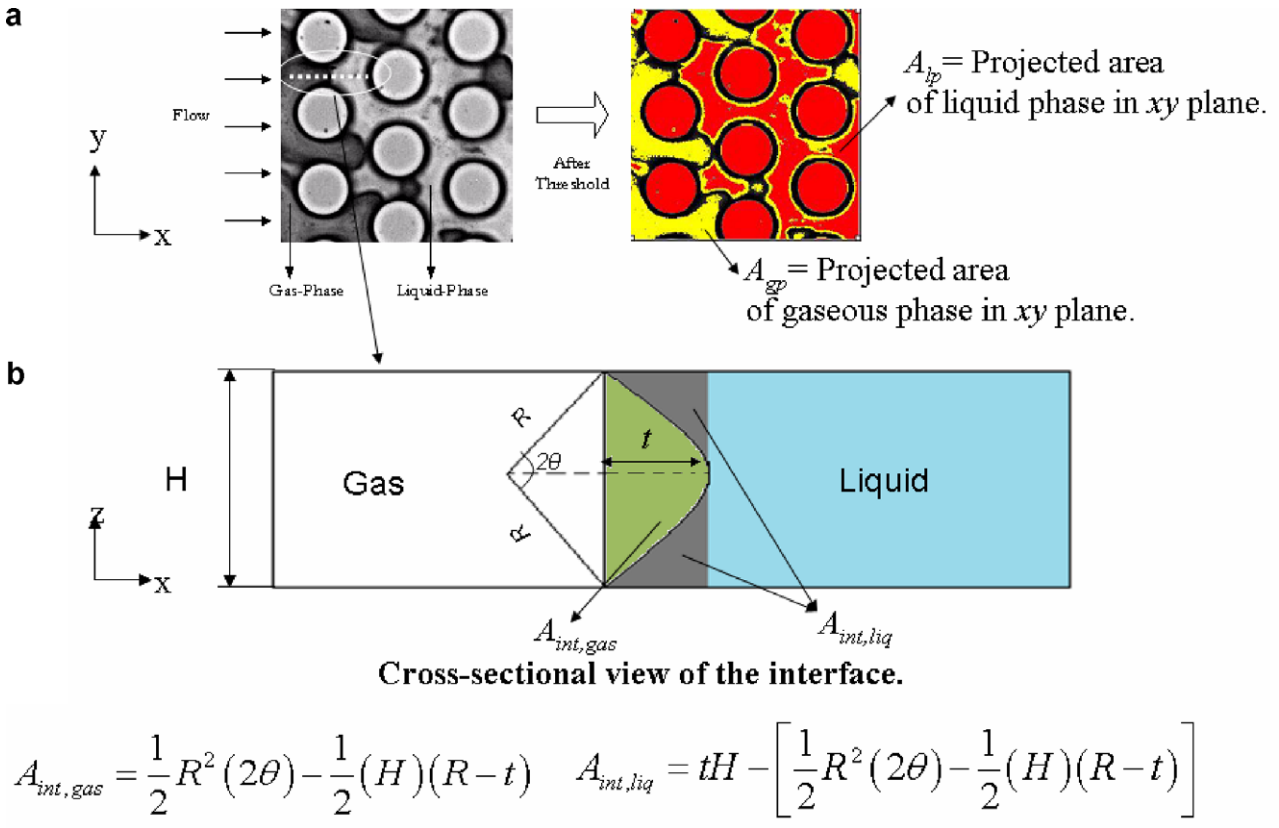

$$A_{int,gas} = \frac{1}{2}R^2(2\theta) - \frac{1}{2}(H)(R-t) \qquad A_{int,liq} = tH - \left[\frac{1}{2}R^2(2\theta) - \frac{1}{2}(H)(R-t)\right]$$

Fig. 3. Schematic showing the methodology for determining the void fraction.

Table 1
Uncertainty in variables

Uncertainty variables	Error (%)
Flow rate, Q (for each reading)	1
Inlet and exit pressures	0.25
Tube hydraulic diameter, D	1
Channel width, w	1
Channel height, H	0.67
Density of fluid, ρ_l	0.5
Void fraction, α	4
Mass flux, G	3.8
Reynolds number, Re	4
Frictional multiplier, ϕ_l^2	3–10
Interfacial friction, f_i	2.5–12

using the propagation of the uncertainty method by Kline and McClintock (1953).

3. Data reduction

3.1. Single phase flow

The single-phase friction factor, f, is obtained according to:

$$f = \frac{2[P_i - P_o]\rho_l}{NG^2}, \tag{3}$$

where P_i and P_o are the inlet and outlet pressures, ρ_l is the liquid density, N is the total number of rows, and G the mass flux, defined as:

$$G = \frac{Q\rho_l}{A_{\min}}, \tag{4}$$

where Q is the volumetric flow rate, and $A_{\min}$ is the minimum cross-sectional flow area, which for the current staggered pillar device with a transverse pitch, S_T, and diagonal pitch, S_D, is given by:

$$A_{\min} = \frac{S_T - D}{S_T} wH \text{ for } \frac{S_T + D}{2} < S_D, \tag{5}$$

where w is the width of the channel and H is the height of the channel. Pressure drop data for different flow rates are recorded and the corresponding friction factor is elucidated for each single-phase Reynolds number defined as $Re_d = Gd/\mu_l$ using the following equation:

$$f = a(Re_d)^{-n}. \tag{6}$$

3.2. Two-phase flow

The measured two-phase pressure drop consists of two components, namely, frictional (ΔP_f) and acceleration (ΔP_{acc}) terms:

$$\Delta P_{\text{measured}} = \Delta P_f + \Delta P_{\text{acc}}. \tag{7}$$

The frictional pressure drop is calculated once the acceleration term is determined by the following equation (Kawahara et al., 2002; Carey, 1992):

$$\Delta P_{\text{acc}} = \left\{\frac{G^2x^2}{\rho_g\alpha} + \frac{G^2(1-x)^2}{\rho_l(1-\alpha)}\right\}_{\text{outlet}} - \left\{\frac{G^2x^2}{\rho_g\alpha} + \frac{G^2(1-x)^2}{\rho_l(1-\alpha)}\right\}_{\text{inlet}}, \tag{8}$$

where α is the time averaged experimental void fraction and x is the mass quality. The Martinelli parameter, X_{vv}, used for correlating the frictional multiplier, $(\sigma_l)^2$, is calculated as:

$$X_{vv} = \left[\frac{(\Delta P_f/\Delta Z)_l}{(\Delta P_f/\Delta Z)_g}\right]^{1/2}, \tag{9}$$

$$(\Delta P_f)_l = \frac{Nf[G(1-x)]^2}{2\rho_l}, \tag{10}$$

$$(\Delta P_f)_g = \frac{Nf[Gx]^2}{2\rho_g}. \tag{11}$$

4. Results and discussion

4.1. Flow patterns and transition

Similar to water, four primary flow patterns were observed: bubbly-slug, gas-slug, bridge, and annular flows. (For more details on their description and formation mechanisms, the reader is referred to Krishnamurthy and Peles, 2007.) Flow map for ethanol as a function of superficial gas and liquid Reynolds numbers with the corresponding transition lines for water is shown in Fig. 4. As can be observed, the flow pattern transition lines were different for the two fluids. The lower surface tension of ethanol resulted in the presence of bubbles whose characteristic size were smaller than the spacing between the pillars (Fig. 5a) – unlike the results for water. This delayed the transition from bubbly flow to gas-slug flow for ethanol. At high liquid Reynolds numbers the transition to bridge flow was delayed for ethanol. Bridge flow pattern was observed when long gas slugs coalesced and resulted in the formation of gas core with liquid bridges between the pillars. The lower surface tension of ethanol shortened the gas slugs and caused them to break. With increasing gas velocity, they coalesced and transitioned to bridge flow. Fig. 5(b) also shows the flow patterns close to the transition lines. As discussed by Krishnamurthy and Peles (2007), the transition to annular flow occurred when the liquid bridges broke. Since the bridges in ethanol were held together by weaker surface tension forces compared to water, the transition to annular flow occurred at lower gas Reynolds number.

4.2. Void fraction

Fig. 6 shows the variation of void fraction along the channel length for various gas and liquid superficial velocities. As shown, the variation is longitudinal direction is insignificant, suggesting that the flow is fully developed within the first few rows of micro pillars. Fig. 7 compares the variation of void fraction with mass quality for ethanol and water along with values predicted by the homogeneous model (Carey, 1992). The void fractions for water and ethanol were considerably lower than prediction from the homogenous model indicating that considerable slip existed between the phases. It can also be observed that at intermediate qualities ($0.04 < x < 0.1$), the void fraction depended on surface tension – void fraction was higher for ethanol than water. This can be attributed to the presence of bridge and gas slug flows, whose formation and transition mechanisms depend on surface tension (Krishnamurthy and Peles, 2007). For ethanol the bridges broke at lower superficial gas velocities than for water, which increased the void fraction. On the other hand, for water at low void fraction, the presence of bridges modified the gas flow path. Furthermore, the void fraction of water also showed mass flux dependency at intermediate qualities unlike the results for ethanol. At higher and lower qualities, the deviations of the void fraction between ethanol and water were negligible, primarily because the dominant flow patterns in these regions were bubbly-slug and annular flows, both of which are governed by shear forces. Since ethanol and water have comparable viscosities, the void fractions were similar in these regions. Based on the above discussion it appears that the void fraction was not strongly dependent on the surface tension, but similar to conventional scale systems, depended on the density and viscosity ratios of the two-phases. This concurs with the results of Kawahara et al. (2005) that suggests that the void fraction in microchannels does not depend on surface tension. While the surface tension can implicitly affect the void fraction – it can alter the flow morphology, which in turn affects the slip ratio between the phases – this effect seems to be much less dominant in the condition of the current study since the viscosity and density of both liquids are quite similar. Therefore, the void fractions for both liquids have been correlated with single-phase friction factor, f, and mass quality, x, similar to Krishnamurthy and Peles (2007):

$$\frac{\alpha}{\alpha_h} = 1 + A(f)^B \ln(x), \tag{12}$$

where the constants A and B are empirically fitted constants, which where found to be 0.0388 and 0.25 and α_h is the homogenous void fraction. Ninety percent of the predicted data fell within 15% of the experimental data as shown in Fig. 8.

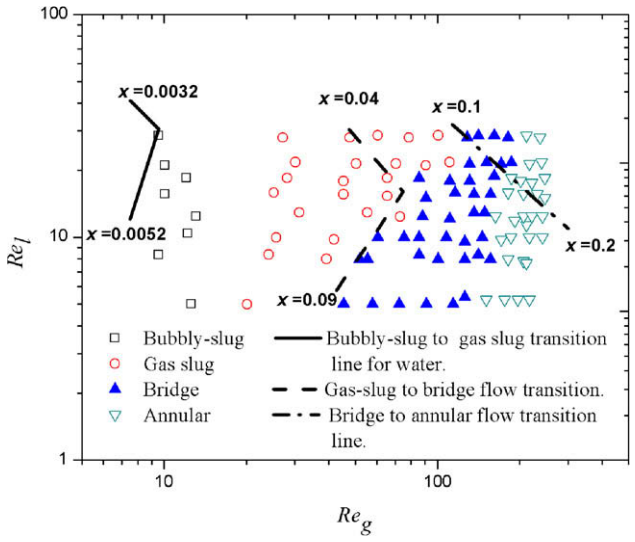

Fig. 4. Comparisons the ethanol flow map with the transition lines for water obtained by Krishnamurthy and Peles (2007).

4.3. Pressure drop

The single-phase friction factor was compared with available tube bundle correlations (Table 2). As shown in Fig. 9, existing correlations agree well with the experimental results at high Reynolds numbers. At low Reynolds numbers the friction factor for the micro pin fins are considerably larger than the prediction obtained from the correlations (Koşar and Peles, 2006). Similar discrepancy was also observed by **?**), Prasher et al. (2007), and Siu-Ho et al. (2007) for flow across micro pin fins and was attributed to end-wall effects, which resulted in the thickening of the boundary layer and a delay in flow separation.

Fig. 10 shows the variation of the dimensionless two-phase pressure drop ($\Delta P/\rho_l j_l^2$) with respect to the superficial gas Reynolds number for water and ethanol. Two regions of different slopes were evident for both fluids. The change in the slope can be attributed to the change in the flow patterns. The region of low superficial gas Reynolds numbers corresponded to bubbly-slug and gas-slug flows; the region of moderate and high gas Reynolds numbers corresponded to bridge flow; and the region of high Reynolds numbers corresponded to annular flow. It can also be observed that the dimensionless pressure drop for ethanol was lower than that of water, which can be attributed to the detailed flow pattern characteristics resulting from the lower surface tension of ethanol. A crude estimate suggests that surface tension forces have negligible effect on the total pressure drop. It appears that the prime cause for the observed increase in the pressure drop of the water was flow morphology modification, which forced the gas slugs to move in a serpentine pattern. This in turn, increased the flow length and as a result the frictional pressure losses. Additionally, due to the small length scale of the current device, it is also possible that interfacial friction between the gas and liquid phases may be significant in the reduction of the two-phase pressure drop for ethanol.

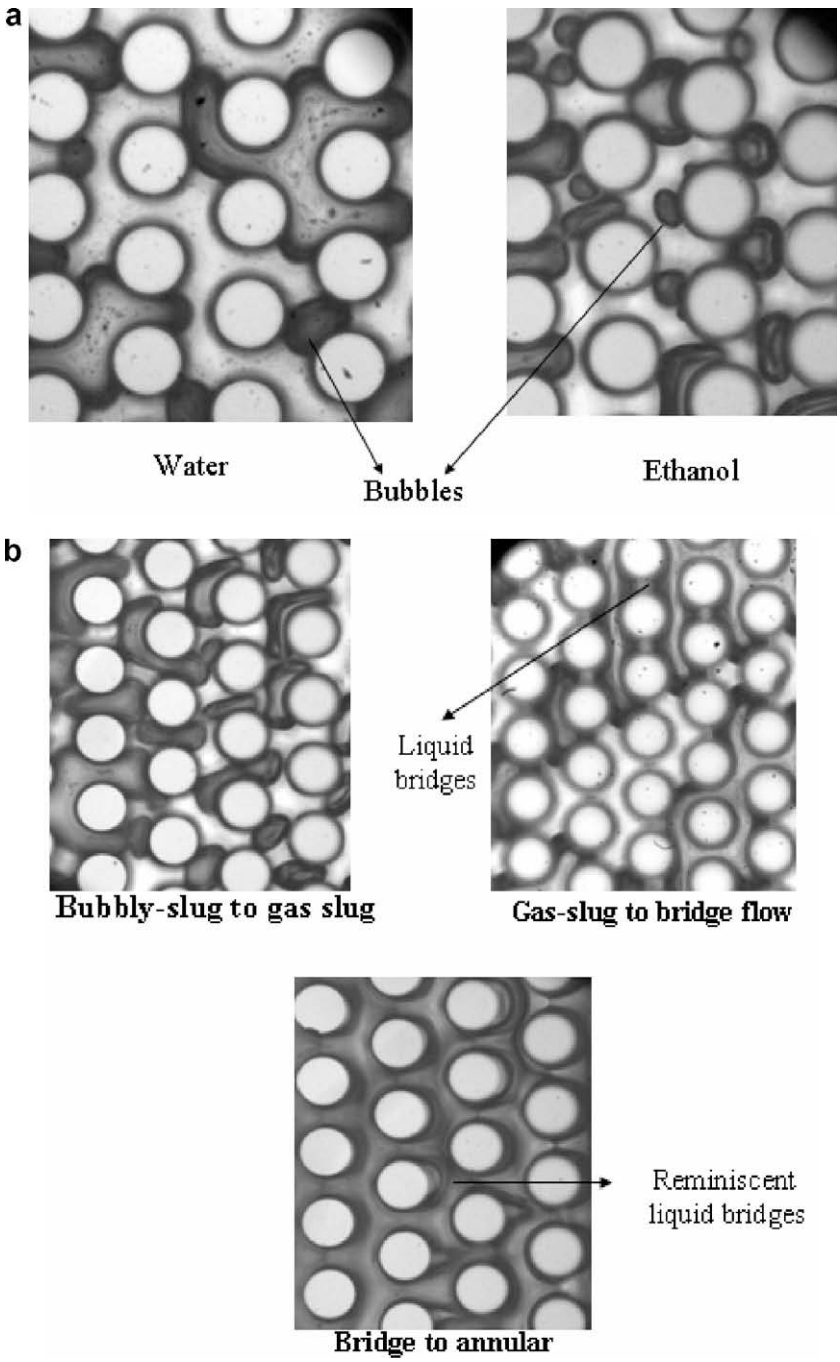

Fig. 5. (a) Bubbles in water and ethanol. (b) Flow patterns close to the transition lines.

Ishii and Zuber (1979) proposed a two-fluid model for in-tube flows at low qualities, which has been used to model the interfacial friction forces between the gas and liquid phases. This approach is based on the mass, momentum, and energy balance and was used for determining the local conditions like void fraction and velocity for the liquid and gas phases. This method was later extended to shell-side flows (Rahman et al., 1996; Gebbie and Jensen, 1997; Edwards and Jensen, 1991; Simovic et al., 2007) taking into account the relative velocity between the phases, which was larger than for in-tube flow.

The use of concepts and relations that were originally introduced for flow in-tubes has been widely employed by many to flow over an array of bluff bodies, such as tube bundle and pin fins, to a large degree of success. Since flow over an array of tube bundles or pin fins can be much more complicated than flow in straight tubes, adaptation of in-tube concept and correlations might not be sufficient to fully divulge the underlining physics. However, it provides a good basis to identify important processes controlling the flow. Therefore, a similar approach was applied in the current study, because of the inherent slip that existed between the phases and the similarity in flow configuration. Since the flow was adiabatic, there was no acceleration and the void fraction was assumed to be constant along the channel, both in the longitudinal and the transverse directions. Therefore, a one-dimensional modeling approach was adopted.

The first step in developing a correlation for interfacial friction using the two fluid model requires the determination of the porosity (ψ) – the ratio of volume accessible to the flow per unit volume (Fig. 11):

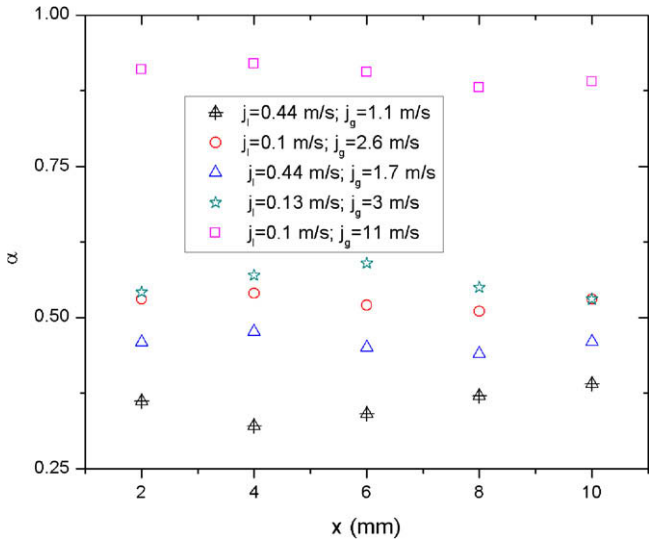

Fig. 6. Void fraction variation along the channel length.

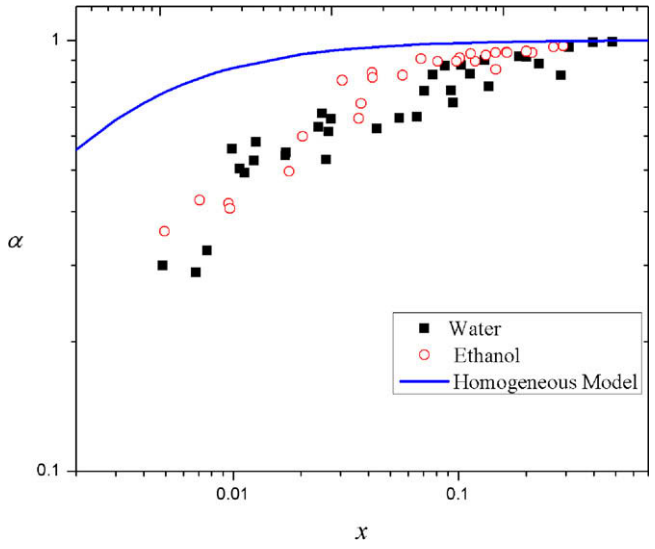

Fig. 7. Void fraction as a function of mass quality for water and ethanol.

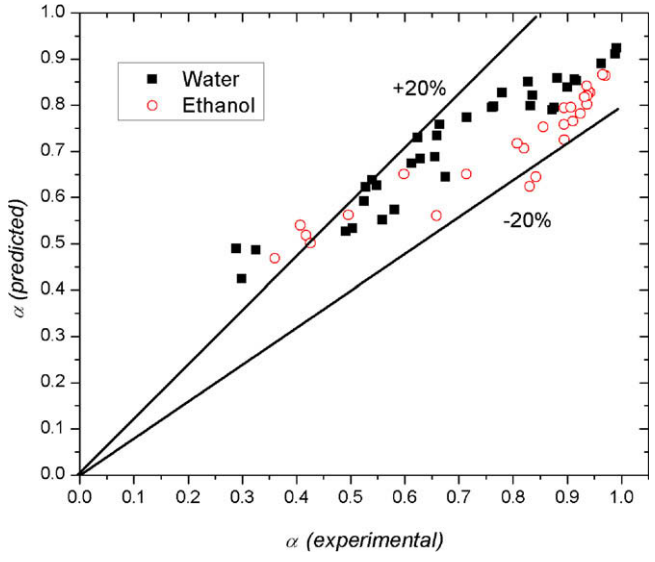

Fig. 8. Comparison between experimental data and prediction from the correlation.

$$\psi = 1 - \frac{\pi D^2}{4 S_T S_L}, \tag{13}$$

where D is the diameter of the pillar The momentum transfer due to interfacial friction depends on the interface topography and on the interfacial shear stress (τ_i). The interfacial friction force acting on the gas phase is given by:

$$F_d = \tau_i A_g, \tag{14}$$

where A_g is the cross-sectional area of the gas phase in the control volume. Substituting for interfacial shear stress, Eq. (14) reduces to:

$$F_d = \frac{1}{2} f_i \rho_m v_r^2 A_g, \tag{15}$$

where f_i is the coefficient of interfacial friction, ρ_m is the mixture density (defined based on the void fraction and incorporate the effect of slip) expressed as $\rho_m = \alpha\rho_g + (1-\alpha)\rho_l$, and v_r is the relative velocity between the gas and liquid phase. The interfacial friction force, F_d, can also be expressed in terms of the interfacial friction, f_{gv}:

$$F_d = f_{gv} V, \tag{16}$$

where V is the volume. Equating Eq. (16) to Eq. (15) and rearranging:

$$f_i = \frac{2 f_{gv} V}{A_g \rho_m v_r^2}, \tag{17}$$

Using the void fraction definition:

$$\alpha = \frac{A_g}{A} = \frac{V_g}{V}, \tag{18}$$

V/A can be expressed as:

$$\frac{V}{A} = \frac{V_g}{A_g} = \frac{\alpha S_T S_L H \psi}{\alpha S_T H \psi}. \tag{19}$$

Substituting for V in Eq. (17) gives:

$$f_i = \frac{2 f_{gv} S_L}{\alpha \rho_m (v_g - v_l)^2}. \tag{20}$$

The gas and liquid velocities in the above equation can be calculated as:

$$v_l = \frac{G(1-x)}{\rho_l (1-\alpha)\psi}, \tag{21}$$

and

$$v_g = \frac{Gx}{\rho_g \alpha \psi}. \tag{22}$$

The momentum balance for the gas-phase can be written similar to Rahman et al. (1996) as follows:

$$\alpha \frac{dp}{dz} + f_{gl} + f_{gw} = 0, \tag{23}$$

where f_{gw} is the specific gas-wall frictional force. Since the flow was adiabatic, it was assumed that the gas was not in contact with the sidewalls (i.e., a thin liquid film between the gas and the walls of the channel existed). Therefore, f_{gw} is null. Substituting Eq. (23) into Eq. (20) with $f_{gw} = 0$ gives the interfacial friction (f_i):

$$f_i = \frac{2 \frac{dp}{dz} S_L}{\rho_m (v_g - v_l)^2}. \tag{24}$$

The interfacial friction is generally correlated in terms of pertinent nondimensional parameters, which are dependent on the flow characteristics and configuration. For example, Ishii and Zuber (1979) correlated their interfacial friction for in-tube flows in terms of the Reynolds number, which was expressed in terms of the liquid density, bubble diameter, relative velocity, and mixture viscosity

Table 2
Friction factor correlations

Sl no	Reference	Geometry	Flow regime	**Correlation**
1	Gunther and Saw (1945)	Circular tubes	Laminar	$f=\frac{180}{Re}\left(\frac{4S_TS_L}{\pi D^2}-1\right)^{0.4}\left(\frac{S_d}{D}\right)$
2	Gaddis and Gneilski (1985)	Circular tubes	Laminar	$f=\frac{280\pi\left(\left(\left(\frac{S_L}{D}\right)^{0.5}-0.6\right)^2+0.75\right)}{Re\left(\frac{4S_TS_L}{D^2}-\pi\right)\frac{S_d}{D}}$
3	Short et al. (2002)	Circular tubes	$Re<1000$	$f=140.4\left(\frac{S_L}{D}\right)^{-1.3}\left(\frac{S_T}{D}\right)^{-0.78}\left(\frac{H}{D}\right)^{-0.55}Re^{-0.65}$
4	Chilton and Generaux (1933)	Circular tubes	Laminar	$f=\frac{106}{Re}$

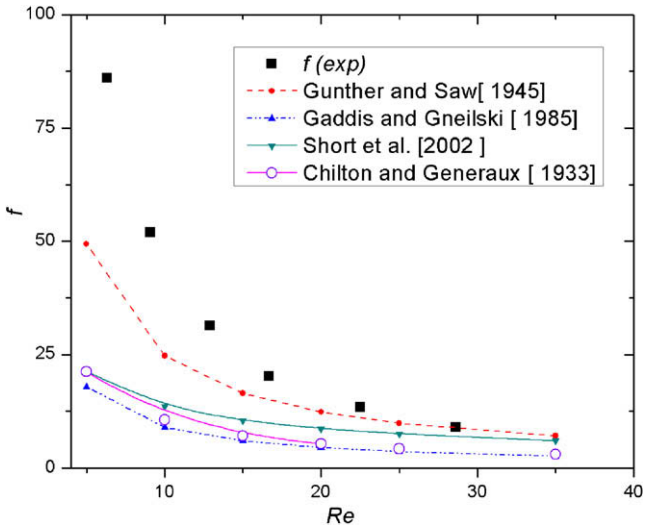

Fig. 9. Comparison of experimentally determined friction factors with various conventional scale correlations.

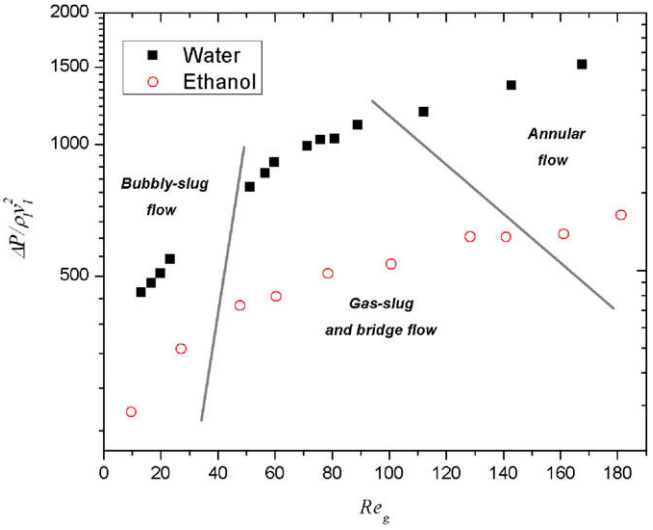

Fig. 10. Variation of non-dimensional pressure drop with gaseous Reynolds number.

(in terms of the void fraction). Rahman et al. (1996) correlated the interfacial friction for the data obtained by Dowlati et al. (1990) for adiabatic two-phase flow across a bank of tube bundles, using a modified Reynolds number defined as a function of the void fraction and the respective velocities of the two phases. Using the bubble diameter as the characteristic length scale for the Reynolds number in the current study was not appropriate, because purely bubbly flow was not observed, and a wide range of bubble diameters existed. Thus, the modified Reynolds number (Re_{tp}) was defined similar to one by Rahman et al. (1996):

$$Re_{tp}=\frac{\rho_m v_r \psi S_L}{\mu_l}. \tag{25}$$

Fig. 12 shows the variation of the interfacial friction as a function of the modified Reynolds number for water and ethanol. The interfacial friction factor for ethanol was lower than for water, but for both fluids it decreased asymptotically with increasing Reynolds number. This is consistent with the Blasius-type relation of the friction coefficient in single-phase flows. At low Reynolds number, higher viscous forces, existing between the gas and liquid interface, resulted in higher interfacial friction. With increasing Reynolds number, the slip between the phases increased and as a result, the interfacial friction, which varies inversely with the relative velocity, $v_r = v_l(S\text{-}1)$, decreased. Besides the direct dependency of the viscous forces on the Reynolds number, at higher Reynolds number, a mass flux dependency of the interfacial friction was also observed. Based on the above mentioned dependency of the interfacial friction on various parameters, the following correlation was proposed:

$$f_i = ARe_{tp}^b\left(\frac{\sigma_w}{\sigma}\right)^c Re_l^d, \tag{26}$$

where σ and σ_w is the surface tension of any fluid and water, respectively and Re_l is the liquid only Reynolds number based on the pillar diameter. A, b, c, and d are empirically derived constants, which were obtained by fitting 186 datum points by means of regression analysis and were found to be 512, −1.94, −0.49, and 0.605, respectively. Fig. 13 shows that the above correlation is able to predict the data within ±15% of the experimental data.

4.4. Two-phase frictional multiplier

Fig. 14 shows the variation of the frictional multiplier as a function of the Martinelli parameter. For a given Martinelli parameter, the frictional multiplier increased with increasing liquid Reynolds number. Similar variation was observed for water by Krishnamurthy and Peles (2007). Fig. 15 compares the experimental results of the frictional multiplier for ethanol with the correlation developed by Krishnamurthy and Peles (2007) for water for similar flow configuration. The correlation over predicted the experimental results. As discussed above, the observed effect can be attributed to the reduction in the interfacial friction due to surface tension. Thus, to account for surface tension, the following correlation for the frictional multiplier is proposed:

$$(\phi_l)^2 = 1+\frac{B\left(\frac{\sigma}{\sigma_w}\right)^a Re_l}{X_{vv}}+\frac{\left(\frac{\sigma}{\sigma_w}\right)^c}{X_{vv}^2}, \tag{27}$$

where B, a, and c are empirically derived constants, which were obtained by fitting the data using regression analysis and were found

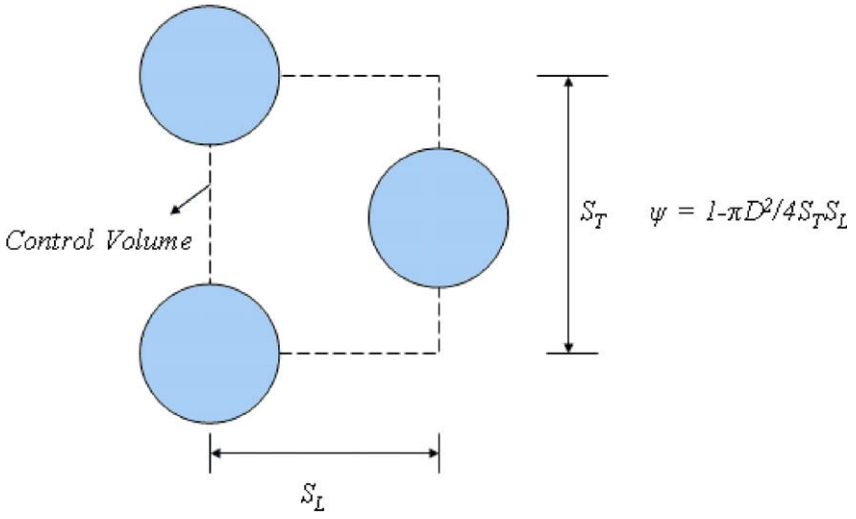

Fig. 11. Schematic showing the staggered arrangement and porosity.

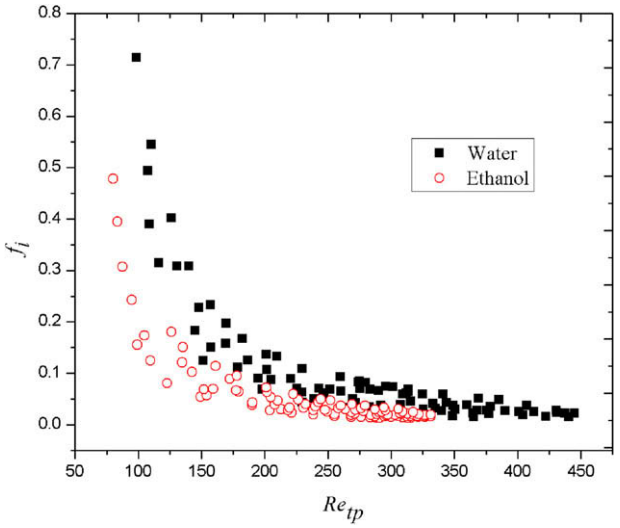

Fig. 12. The variation of interfacial friction with two-phase Reynolds number.

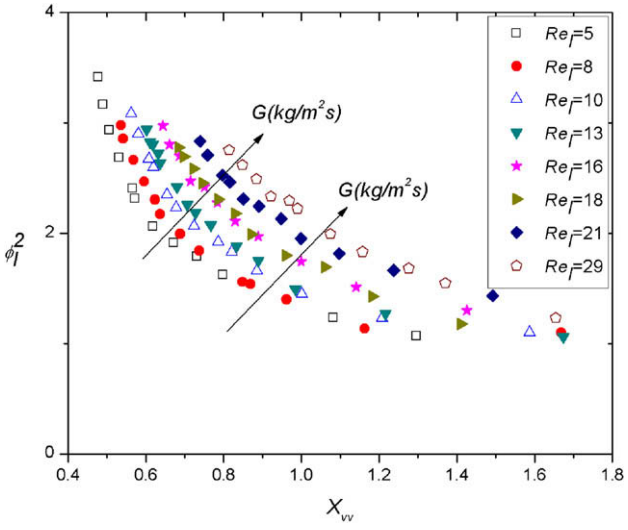

Fig. 14. Variation of frictional multiplier with Martinelli parameter.

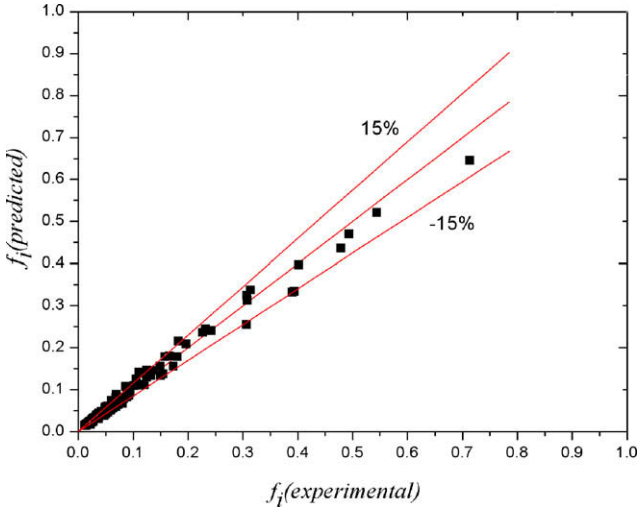

Fig. 13. Comparison of experimental data with the new correlation.

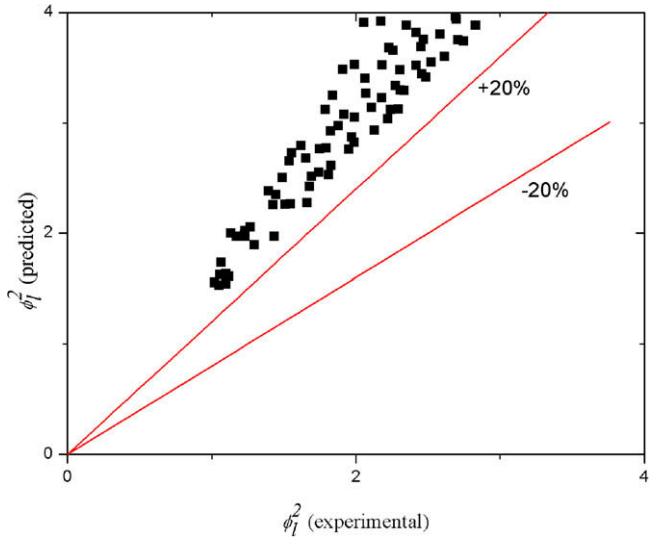

Fig. 15. Comparison of the experimental data with the predicted data from the correlation derived by Krishnamurthy and Peles (2007).

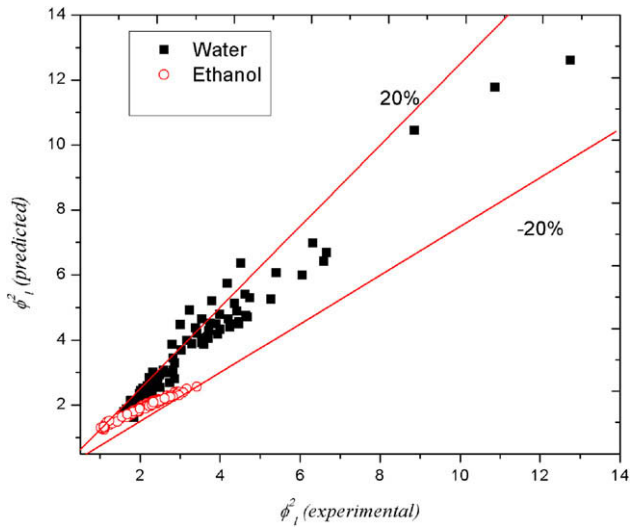

Fig. 16. Comparison between experimental data and prediction from Eq. (27).

to be 0.0358, −0.094, and 1.1, respectively. A total of 90% of the predicted data falls within ±20% of the experimental data and provided a MAE of 15% (Fig. 16).

5. Conclusion

The effect of surface tension on two-phase flow characteristics such as flow morphology, void fraction, and two-phase pressure drop was studied. The main conclusions derived from this study are:

- No significant deviations were observed between water and ethanol with respect to flow patterns. However, the reduction of surface tension affected the flow pattern transition lines.
- The void fraction results for water and ethanol were compared and were found to be a weak function of surface tension. The void fraction is more sensitive to liquid density and viscosity. The void fraction correlation suggested by Krishnamurthy and Peles (2007) was, thus, used to predict the experimental data of ethanol and good agreement was obtained.
- Slope change in pressure drop vs. gas Reynolds number curve suggested that flow patterns affected the pressure drop characteristics. Furthermore, the two-phase pressure drop for water was found to be higher than for ethanol, signifying the effect of flow pattern transition on the pressure drop.
- Relation for interfacial friction coefficient was derived using the method suggested by Rahman et al. (1996). The coefficient of interfacial friction was found to be a function of surface tension ratio of the liquids (water and ethanol) and a correlation was developed incorporating this effect. The resulting correlation was able to predict the data with MAE of 10%.
- The correlation developed by Krishnamurthy and Peles (2007) was modified to account for the effect of surface tension on pressure drop. The resulting correlation was able to predict the combined experimental data of water and ethanol to within ±10%.

Acknowledgements

This work was supported by the Office of Naval Research (Program Officer: Dr. Mark Spector). Graduate student support from Rensselaer Polytechnic Institute is also gratefully appreciated. The microfabrication was performed in part at the Cornell Nano-Scale Facility (a member of the National Nanotechnology Infrastructure Network) which is supported by the National Science Foundation under Grant ECS-0335765, its users, Cornell University and industrial affiliates.

References

Carey, V.P., 1992. Liquid–Vapor Phase-Change Phenomena. Taylor & Francis.
Chisholm, D., Laird, A.D.K., 1949. Two-phase flow in rough tubes. Trans. ASME 80, 276–286.
Christel, L.A., Peterson, K., McMillan, W., Northrup, M.A., 1999. Rapid automated nucleic acid prob assays using silicon microstructures for nucleic acid concenteration. J. Biomech. Eng. 121, 22–27.
Chilton, T.H., Generaux, R.P., 1933. Pressure drop across tube banks. Trans. Am. Ins. Chem. Eng. 29, 161–173.
Chung, P.M.-Y., Kawaji, M., 2004. The effect of channel diameter on adiabatic two-phase flow characteristics in microchannels. Int. J. Multiphase Flow 30, 735–761.
Cubaud, T., Ho, C.-M., 2004. Transport of bubbles in square microchannels. Phys. Fluids 16, 4575–4585.
Dowlati, R., Kawaji, M., Chan, A.M.C., 1988. Void fraction and friction pressure drop in two-phase flow across a horizontal tube bundle. AICHE Symp. Ser. 184, 126–132.
Dowlati, R., Kawaji, M., Chan, A.M.C., 1990. Pitch-to-diameter effect on two-phase flow across an in-line tube bundle. AICHE J. 36 (5), 765–772.
Dowlati, R., Chan, A.M.C., Kawaji, M., 1992b. Hydrodynamics of two-phase flow across horizontal in-line and staggered rod bundle. J. Fluids Eng. 114 (3), 450456.
Edwards, D., Jensen, M., 1991. A two-dimensional numerical model of two-phase heat transfer and fluid flow in kettle boilers. ASME HTD 159, 9–16.
Field, B.S., Hrnjak, P., 2007. Adiabatic two-phase pressure drop of refrigerants in small channels. Heat Transfer Eng. 28 (8-9), 704–712.
Gaddis, E.S., Gnielski, V., 1985. Pressure drop in horizontal cross flow across tube bundles. Int. Chem. Eng. 25 (1), 1–15.
Gebbie, J., Jensen, M., 1997. Void fraction distributions in kettle boiler. Exp. Thermal Fluid Sci. 14, 297–311.
Grant, I.D.R., Chislom, D., 1979. Two-phase flow on the shell-side of a segmentally baffled shell-and-tube heat exchanger. J. Heat Transfer 101, 38–42.
Gunter, A.Y., Shaw, W.A., 1945. A general correlation of friction factors for various types of surfaces in cross flow. Mech. Eng. (American Society of Mechanical Engineering) 67, 643–660.
Hitt, D.L., Zakrzwski, C.M., Thomas, M.A., 2001. Mems-based satellite micropropulsion via catalyzed hydrogen peroxide decompsition. Smart Mater. Struct. 10, 1163–1175.
Ishii, M., Zuber, M., 1979. Drag coefficient and relative velocity in bubbly, droplet or particulate flows. J. AIChE 25, 843–855.
Kawahara, A., Chung, P.M.-Y., Kawaji, M., 2002. Investigation of two-phase flow pattern, void fraction and pressure drop in a microchannel. Int. J. Multiphase Flow 28, 1411–1435.
Kawahara, A., Sadatomi, M., Okayama, K., Kawaji, M., Chung, P.M.-Y., 2005. Effects of channel diamter and liquid properties in adiabatic two-phase flow through microchannels. Heat Transfer Eng. 26 (3), 13–19.
Kawaji, M., Chung, P.M.Y., 2004. Adiabatic gas–liquid flow in microchannels. Microscale Thermophys. Eng. 8, 239–257.
Kline, S., McClintock, F.A., 1953. Describing uncertainties in single-sample experiments. Mech. Eng. (ASME) 75 (1), 3–8.
Koşar, A., Peles, Y., 2006. Thermal-hydraluic performance of MEMS based pin fin heat sink. J. Heat Transfer 128, 121.
Koşar, A., Peles, Y., 2007. Boiling heat transfer in a hydrofoil-based micro pin fin heat sink. Int. J. Heat Mass Transfer 50 (5-6), 1018–1034.
Krishnamurthy, S., Peles, Y., 2007. Gas–liquid two-phase flow across a bank of micro pillars. Phys. Fluids 19 (4), 043302–043314.
Krishnamurthy, S., Peles, Y., 2008. Two-phase flow pattern transition across micro-pillars size scale effect at the micro scale. Phys. Fluids 2, 023602.
Lee, H., Lee, S., 2001. Pressure drop correlations for two-phase flow within horizontal rectangular channels with small heights. Int. J. Multiphase flow 27, 783–796.
London, A., 2000. Development and testing of a microfabricated bipropellant rocket engine. Ph.D. thesis, Massachusetts Institute of Technology, Boston, MA.
Losey, M.W., Jackman, J., Firebaugh, S.L., Schmidt, M.A., Jensen, K., 2002. Design and fabrication of microfluidic devices for multiphase mixing and reaction. J. Microelectromech. Syst. 11, 709–717.
Prasher, R., Dirner, J., Chang, J.-Y., Myers, A., Chau, D., He, D., Prstic, S., 2007. Nusselt number and friction factor of staggered arrays of low aspect ratio micropin-fins under cross flow for water as fluid. J. Heat Transfer 129 (2), 141.
Rahman, F.H., Gebbie, J.G., Jensen, M.K., 1996. An interfacial friction correlation for shell side vertical two-phase cross-flow past horizontal in-line and staggered tube bundles. Int. J. Multiphase flow 22 (4), 753–766.
Schrage, D.S., Hsu, J.-T., Jensen, M.K., 1988. Two-phase pressure drop in vertical cross-flow across a horizontal tube bundle. AICHE J. 34, 107–115.
Short Jr., B.E., Raad, P.E., Price, D.C., 2002. Performance of pin fin cast aluminum coldwalls, Part. 1: Friction factor correlations. J. Thermophys. Heat Tr. 16 (3), 389–396.

Simovic, Z.R., Ocokoljic, S., Stevanovic, V.D., 2007. Interfacial friction correlations for the two-phase flow across tube bundle. Int. J. Multiphase flow 33, 217–226.
Siu-Ho, A., Qu, W., Pfefferkorn, 2007. Experimental study of pressure drop and heat transfer in a single-phase micro pin-fin heat sink. J. Electronic Packaging 129, 479–487.
Xu, G.P., Tou, K.W., Tso, C.P., 1998a. Two-phase void fraction and pressure drop in horizontal crossflow across a tube bundle. Trans. ASME 120, 140–155.
Xu, G.P., Tso, C.P., Tou, K.W., 1998b. Hydrodynamics of two-phase flow in vertical up and down-flow across a horizontal tube bundle. Int. J. Multiphase Flow 24, 1317–1342.